Spray Characteristics and Vaporization process of ammonia-ethanol blends with a current Bosch GDI engine injector.

Ronan Pelé, Pierre Brequigny, Camille Hespel, Jérôme Bellettre, Christine Mounaïm-Rousselle

Spray Characteristics and Vaporization process of ammonia-ethanol blends with a current Bosch GDI engine injector

R. Pelé*[1], P. Bréquigny[1], C. Hespel[1], J. Belletre[2], C. Mounïam-Rousselle[1]

[1]Univ. Orléans, INSA-CVL, EA 4229 – PRISME, F-45072 Orléans, France
[2]Laboratoire de Thermique et Energie de Nantes (LTeN UMR Université de Nantes—CNRS 6607)

Abstract
The study aims to provide information on the spray characteristics and vaporization process of ammonia-ethanol blends with a current GDI injector. The Schlieren technique was used to capture images of liquid spray. The penetration length and the spray angle at quarter-penetration length were measured. A part of this study focuses on the vaporization process of the different blends at constant conditions of air density and temperature with a comparison of the modeling of one single droplet vaporization.

Introduction

Using carbon-free energy sources is one of the keys to mitigating climate change. Ammonia is one interesting molecule for efficient and safe hydrogen storage (17.8% by weight) in the liquid phase at approximately 9 bar at 20°C or −34 °C at ambient pressure. Moreover, it is also more and more considered as a zero-carbon fuel for thermal engines or gas turbines. However, its high auto-ignition temperature and research octane number, narrow flammability range, and low laminar flame speed [1] are unfavorable combustion properties. Blending ammonia with more reactive fuels is one solution to improve combustion properties.

Several studies have addressed the potential of ammonia blended with another fuel in internal combustion engines, to promote ignition/combustion properties, as reviewed in Mounaïm-Rousselle and Brequigny [2] and Dimitriou and Javaid [3]. Kurien et al. [4] also reviewed the use of ammonia as an alternate fuel in dual-fuel compression ignition engines. This study demonstrates the effectiveness of ammonia combustion using the dual-fuel approach with secondary fuels like diesel, dimethyl ether, kerosene, and hydrogen. Biofuels, and particularly bio-ethanol, are also another interesting alternative energy sources to contribute to the decarbonization of the transportation sector [5]. Even if the potential of blending ethanol into ammonia is promising due to the perfect solubility between both liquids [6-8], no data are available on the injection process for this kind of blends. Indeed, the injection process is a fundamental aspect especially for internal combustion engine optimization as it allows the control of the in-cylinder air-to-fuel ratio and affects the pollutant emission itself [6]. The objective of the direct injection process is to vaporize as fast as possible the fuel inside the chamber by breaking up the fuel spray into droplets. Then, the vaporization of droplets is greatly significant for the spatial distribution of fuel vapor/air, the ignition, and the combustion itself. Generally, the use of high-pressure injection systems [7] favors the atomization in small droplets which enhances the liquid-air interface, the vaporization, and the fuel/air mixing [8], [9]. The effects of injection pressure on droplet size reduction become limited or even disappear when the injection pressure reaches a threshold [7]. Another possibility to reduce droplet size is the flash boiling condition itself, which produces finer droplets and a more uniform fuel/air mixture [11]. Flash boiling is a thermodynamic state of fuel spray that occurs when a subcooled liquid is rapidly depressurized to a pressure below its liquid saturation pressure [10].

By adding ethanol into ammonia generates an effervescent atomization due to their high difference in vapor pressures : $P^{Sat}_{C_2H_5OH}(293K) = 5.4kPa$ and $P^{Sat}_{NH_3}(293K) = 855.8kPa$, [11][12] thus potentially improving the ethanol vaporization when the pressure is below the saturation pressure of ammonia during the direct injection.

In this experimental study, the spray characteristics of ammonia/ethanol blends under different ammonia ratios, at constant air density and temperature were investigated in a constant-volume chamber. The Schlieren technique was used to capture images of liquid spray. The penetration length and the spray angle at quarter-penetration length were measured. A part of this study focuses on the vaporization process of the different blends at a fixed condition of air density and temperature by a comparison with the modeling of one single droplet vaporization as in [4].

Experimental set-up

A constant volume 2.5 L chamber was used to follow the spray development. As described in [13], it can be pressurized to the desired pressure up to 30 bar by an air compressor and warmed up to 200 °C by wall

* Corresponding author: ronan.pele@etu.univ-orleans.fr

heating resistances. Between each spray, the chamber is purged with flushed air that is vented to the outside. All the different blends are pressurized up to 120 bar by pressurized Helium. A current gasoline direct Bosch injector (7 holes of 150 µm diameter) is used to generate the spray. The temperature and injection duration are controlled through an automation system driven by a Labview program. The pressure and the temperature are measured by a pressure sensor from KELLER (PAA-33X model) and a T thermocouple, respectively with a precision of 4mbar and 0.1K respectively.

Schlieren Setup

The Schlieren technique, based on the measurement of the deviation of the light source through the test section, was used to follow the liquid development. This high sensitivity to refractive index gradients makes it possible to identify the limit of the line of sight between the liquid fuel and the ambient gases [14]. The sensitivity is a function of the light intensity and is adjustable by a diaphragm in front of the camera; a small diaphragm opening increases the sensitivity. Figure 1 presents a scheme of the optical setup: two concave mirrors (f = 863.6 mm, d = 108 mm) are mounted in front of the optical windows of the chamber at 57 cm (N°2, Figure 1) and 84 cm (N°5, Figure 1). A 538 nm light beam from a LED (HardSoft DLR IL104G) passes through the concave mirror, crosses the chamber, and by means of another concave mirror passes through a diaphragm.

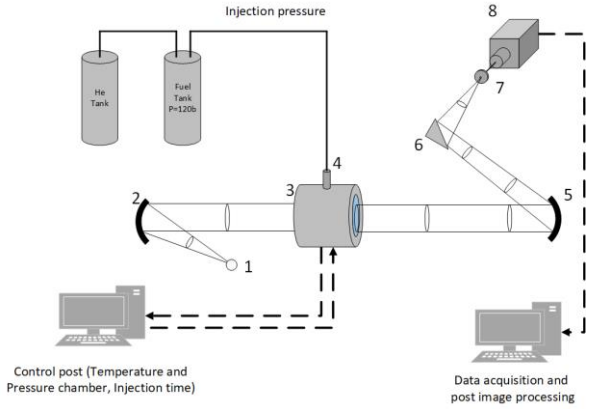

Figure 1. Scheme of the experimental and optical setup; 1 Light ED source; 2 and 5 Concave mirrors; 3 Chamber; 4 Injector; 6 Plane mirror; 7 Adjustable diaphragm; 8 CMos FastCam (High-speed camera).

The images are recorded at 15,000 frames per second with a CMos high-speed camera (FastCam SA5, Photron), associated with a 105 mm Nikkon camera lens, to reach an image resolution of 768 × 648 pixels^2, with a spatial resolution of 0.160 mm/pixel.
For each operating condition, 100 images were recorded, and each experiment was repeated 10 times.

Image Post-Processing

Post-processing of 100 raw images was performed in several steps in a Matlab environment. The first six raw images were used to generate an average background. After subtraction of this average background and inversion, the image was binarized using the Otsu's method for thresholding [15]. To simplify the calculation of spray penetration and the different angles, the binarized image was rotated. On the rotated image, spray penetration length (SP) and spray angle at 1/4 SP were calculated, as visible in Figure 2.

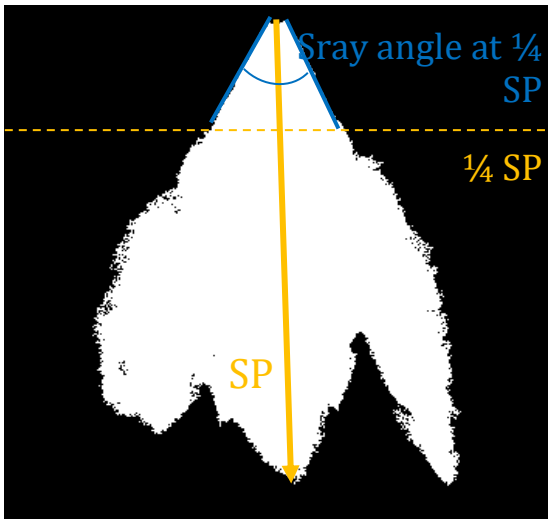

Figure 2. Definition of spray characteristics for the liquid spray of ethanol as an example

SP is the distance between the injector and the end of the spray. The spray angle at 1/4 SP is the value of the angle from the injector outlet to the quarter spray penetration length. Moreover, the area of the spray is measured by summing the white pixel of the binarized image.

Experimental Conditions

The experimental data presented in this study corresponds to the ambient pressure and temperature of 2 bar and 293K. The injection pressure, P_{fuel}, was set at 120 bar and the injection temperature, T_{fuel}, was estimated at 20 °C. Two injection timings are set, the first at 4ms to characterize the spray morphology and the second at 1ms to evaluate the vaporization process.

Four ratios of ammonia/ethanol (25%, 50%, 75%, and 90% of NH_3 by mole defined as X25, X50, X75 and X90) are compared to pure fuels. They are prepared thanks to a mixing set-up using an emulsifier.

Results and discussion

Spray characteristics

The phase state of the mixture is calculated with the equation of state of Peng-Robison using the full methodology described in [16]. Figure 3 shows the Vapor-Liquid Equilibrium (VLE) for ammonia and ethanol blends with the calculated bubble and dew point curves and the experimental conditions.

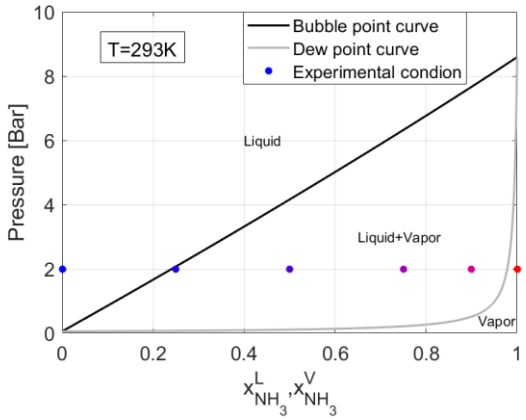

Figure 3. Vapor-Liquid Equilibrium calculation of ammonia/ethanol and experimental conditions

The color range corresponds to the ratio of ammonia in the blend. The blue point, pure ethanol, is in the liquid phase for these ambient P&T conditions. Adding 25% of NH3, the blend is on the limit of the liquid phase. For the blends 50%, 75%, and 90%, fast vaporization will appear due to their liquid+vapor position in the diagram. The pure ammonia, red point, is in the vapor region meaning a flash boiling phenomenon during the injection process.

Figure 4 shows the raw spray images after 1 ms of injection for the different ratios of ammonia. The two images on the left, pure ethanol, and X25, are similar and some of the individual plumes are distinguishably meaning few interactions between them. These weak interactions are mainly due to the liquid state of these mixtures, as seen in Figure 3, thus meaning a slow vaporization process. On the contrary, the pure ammonia spray collapses with a strong plumes-to-plumes interaction. The individual plumes are not visible due to the rapid vaporization. This rapid state change decreases quickly the temperature inside the global spray creating a low-pressure region inside and the plumes get closer. Between these two opposite spray morphologies, three 'transient' spray morphologies are observed. For the ratio of 50%, the individual plumes are not visible but the spray is not collapsed because the spray is large. It can be explained by the fact that ammonia vaporizes at first but the decrease in the temperature inside the spray is not enough cold to collapse the spray. However, when more ammonia is added to the blend, 75% and 90%, the spray collapses with a strong interaction between plumes probably due to a colder temperature inside the spray because of a higher amount of ammonia vaporized.

Figure 5 shows the spray penetration for the different ammonia ratios. Two groups are observed before t=0.75ms with two speeds of spray development. The first one regroups the spray with an ammonia ratio below 50%, also observable in Figure 4. They are characterized by slow evaporation and weak plumes-to-plumes interactions. The second one regroups the spray with a high ammonia ratio characterized by a rapid change of phase state and with a strong collapse effect. However, after t=0.75ms more differences are observed between the blends and the spray development is quicker when more ammonia is added. It can be explained by the collapsing effect that increases the spray penetration speed. The low-pressure zone inside the spray due to the rapid vaporization brings the individual plumes together reducing the friction between the spray and the air.

Figure 6 shows the spray angles at the quarter of the spray penetration length and two behaviors are also observed. A similar angle is measured for all the ammonia ratios before t=0.75ms, nevertheless, after this duration, the same groups of ammonia ratios are formed. The spray angle of the first group is 45° while for the second group, the spray angle is 35°. The sprays are thinner for the high ratio of ammonia due to the collapsing effect, as previously explained.

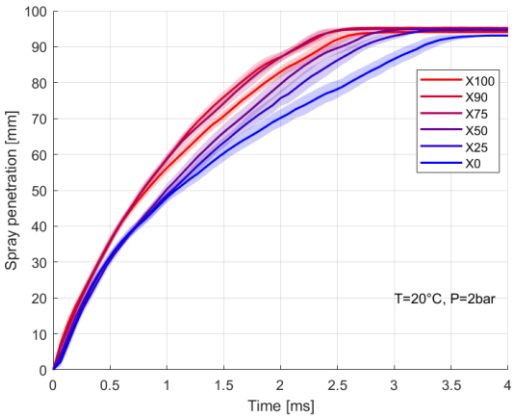

Figure 5. Spray penetration for the different ratio of ammonia

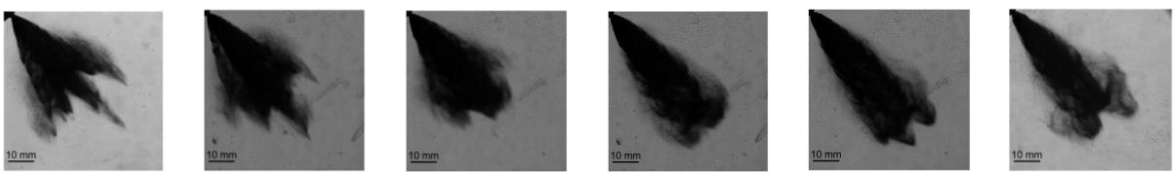

X0 **X25** **X50** **X75** **X90** **X100**

Figure 4. Comparison of spray shape at 1 ms after the start of injection obtained for the different ratio of ammonia at $P_{ambient}$=2bar and $T_{ambient}$=293K, P_{in} =120bar.

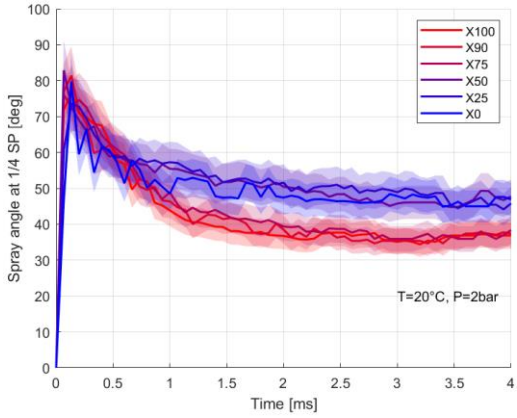

Figure 6. Spray angle at the quarter of the spray penetration for the different ratios of ammonia

Vaporization process

To characterize the vaporization process, the injection duration was reduced to 1 ms and the recorded duration was increased to follow the area of the liquid spray. Figure 7a shows the evolution of the area of the liquid phase for the different ammonia ratios. The black region symbolizes the injection duration and the maximal area is way after the end of the injection time.

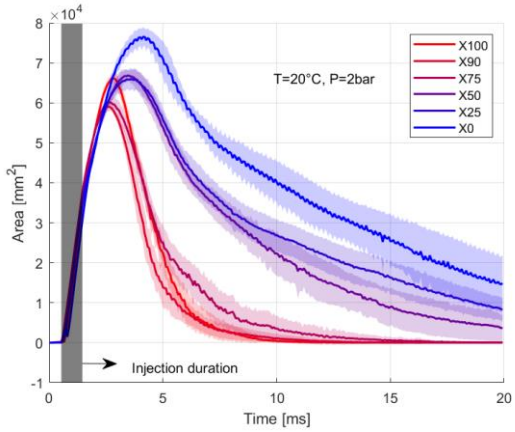

(a)

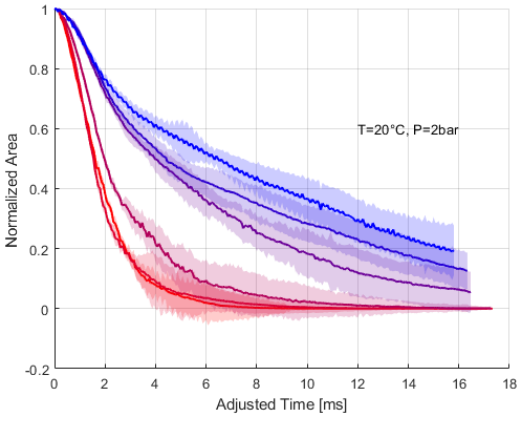

(b)

Figure 7. Evolution of the raw area (a) and the normalized area (b) with an injection duration fixed at 1ms.

Two dynamics of vaporization are clearly distinguishable:

- For pure ammonia and blends with 90% and 75% of ammonia, the spray vaporizes quickly, less than 10ms to be totally vaporized.
- For pure ethanol and blends with only 25 and 50% of ammonia, the spray is still not yet completely vaporized, over 20 ms.

Figure 7b presents the same data but normalized by the maximal area considered as the maximal spray development, as:

$$A_{norm}(t) = \frac{A(t)}{A_{max}} \quad (1)$$

And the time scale is also as below, with t_{max} the time where the area is maximal and $t_{end}$the final recorded time:

$$t_{adjusted} = [0, t_{end} - t_{max}] \quad (2)$$

This plot highlights the effect of adding ammonia into the blend which strongly decreases the vaporization duration but mainly when at least 50% of ammonia is added.

Droplet Vaporization

The droplet vaporization in the same conditions of pressure and temperature was estimated to complete this study and to better understand the process of multicomponent vaporization. The evaporation model used is from [17][18]:

$$\dot{m}_i = -2\pi D_i r_d \rho_{air} \ln(1 + BM_i)\, Sh_i \quad (3)$$

Where $\dot{m}_i$, D_i, r_d, ρ_{air}, BM_i and Sh_i represent respectively the mass flow rate of the specie "i", the diffusion coefficient of the specie "i", the droplet radius, air density, Spalding mass transfer number of the specie "i", and the Sherwood number of the specie "i".

In the case of flash boiling conditions, i.e. when the equilibrium pressure P_{eq} estimated by the Peng-Robinson equation is higher than the ambient pressure, the following model from [19] studying the evaporation of aqueous ammonia droplets was used. Moreover, Cai et al. [20] introduced a corrective factor, φ to take the mass diffusion in the droplet into account in the model:

$$\dot{m}_i = -2\pi r_d M_i D_i Sh_i \left(\frac{x_i^V P_{eq}}{RT_d} - \frac{x_i^\infty P_{amb}}{RT_{amb}} \right) \varphi \quad (4)$$

where x_i^V, x_i^∞ are the mole fraction in the vapor phase of the specie "i" calculated with the Peng-Robinson

equation and the mole fraction far away from the droplet (in this study: $x_i^{\infty} = 0$) , T_d is the droplet temperature.

The heat transfer is considered as followed:

$$mC_p \frac{dT_d}{dt} = h4\pi {r_d}^2 (T_{amb} - T_d) + \sum_{i=1}^{N} \Delta H_i^{Vap} \dot{m}_i \quad (5)$$

Where m is the droplet mass, C_p is the heat capacity of the droplet, h is the heat transfer coefficient and ΔH_i^{Vap} is the latent heat of the specie "i".

The initial conditions of the droplet are: T_d=293K in the ambient conditions P=2bar and T=293K and r_d = 5µm. This radius corresponds to the measurement of droplet size distribution as stated in [21], [22] for the same injector, ambient conditions and injection pressure.

Figure 8.a shows the results of the mass evolution of the droplet and zoom at the start of the calculation enabling to see the change of regime. The flash boiling mode is very short, less than 0.03ms and 14% of the mass is vaporized during this process for the pure ammonia condition. Regarding the temperature evolution, Figure 8.b corresponds to the major part of the temperature drop. Flash boiling is a very short but intense phenomenon.

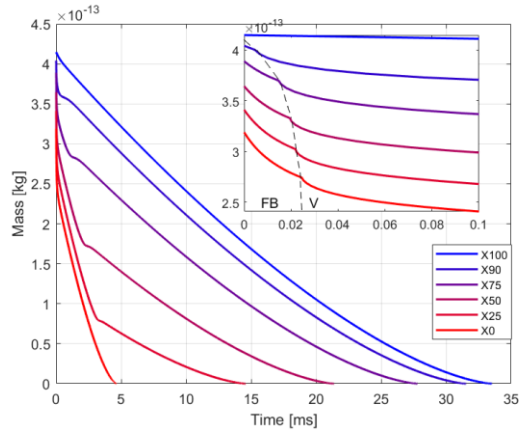

(a)

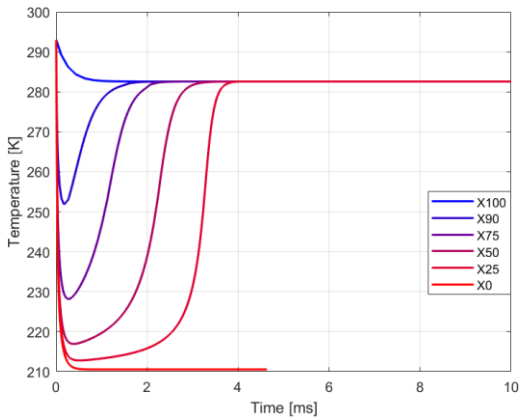

(b)

Figure 8. Mass evolution with a zoom on flash boiling (FB) and the vaporization (V) models (a) and the temperature evolution (b) of the droplets composed of different ammonia ratios

During the vaporization phase, Figure 8.a, two trends of vaporization can be observed between the pure fuels with a slower rate of vaporization for ethanol compared to the pure ammonia. The total duration of evaporation is 7 times higher for ethanol (33.5ms) than for pure ammonia (4.6ms). The different vaporization rate is mainly explained by the difference in the diffusion coefficients: D_{NH_3} =0 .1053.10^{-4} m^2/s and $D_{C_2H_5OH}$=0.0574.10^{-4} m^2/s, twice higher for ammonia. Regarding the blends, a breakpoint is present in their mass evolutions, indicating a change of rate of vaporization. The cause of this change is so that for the blends, ammonia dominates the vaporization and a similar rate of vaporization is observed at the beginning compared to the pure ammonia. However, when all ammonia content is vaporized, only ethanol vaporizes, and the rate of evaporation "switches" to the similar rate of evaporation of ethanol.

To have a significant reduction of evaporation duration more than 50% of ammonia should be added into the blend as experimentally observed, Figure 7.

Figure 8.b, shows the temperature evolution and the equilibrium temperature of ethanol is 282K (9°C) while pure ammonia is 210K (-63°C). This very low temperature is explained by the two different rates of vaporization but also by the difference in latent heat: 877 kJ.kg^{-1} and 1163 kJ.kg^{-1} for ethanol and ammonia respectively. For the blends, the temperature drops due to the ammonia vaporization and then increases to reach the equilibrium temperature of ethanol. It corresponds to the breakpoint seen previously in Figure8.a. As more ammonia is added to the droplet, the temperature becomes colder and tends to reach the equilibrium temperature of ammonia. Moreover, the cold phase is longer when more ammonia is added. A high drop in temperature and a long duration for the cold phase seem necessary conditions to collapse the spray.

Conclusion

The study provides the first information on the spray characteristics and vaporization process of ammonia-ethanol blends with a current engine injector focusing on the conditions of $P_{ambient}$=2bar and $T_{ambient}$=293K. From the Schlieren images, it was concluded that the sprays for pure ammonia and until 25% of ethanol have similar weak plumes-to-plumes interactions due to slow vaporization and a liquid phase state. For 50%ammonia/50%ethanol, it becomes in transient phase. And when the content of ammonia increases until pure ammonia, plumes-to-plumes interaction is stronger with a collapsing effect due to a drop of the temperature inside the spray creating a low-pressure zone. It was pointed out that at least 50% of

ammonia is needed to reduce significantly the vaporization process. The droplet vaporization estimation highlights similar result and provided the indication of droplet temperature drop: from 9°C to -63°C from pure ethanol to pure ammonia, respectively. This low temperature is due to a higher rate of vaporization due to a higher diffusion coefficient for ammonia and higher latent heat.

References

[1] C. Lhuillier, P. Brequigny, F. Contino, and C. Mounaïm-Rousselle, "Experimental investigation on ammonia combustion behavior in a spark-ignition engine by means of laminar and turbulent expanding flames," *Proc. Combust. Inst.*, vol. 38, no. 4, pp. 6671–6678, 2021.

[2] C. Mounaim-Rousselle and P. Brequigny, "Ammonia as Fuel for Low-Carbon Spark-Ignition Engines of Tomorrow's Passenger Cars," *Front. Mech. Eng.*, 2020.

[3] P. Dimitriou and R. Javaid, "A review of ammonia as a compression ignition engine fuel," *Int. J. Hydrogen Energy*, vol. 45, no. 11, pp. 7098–7118, 2020.

[4] C. Kurien and M. Mittal, "Review on the production and utilization of green ammonia as an alternate fuel in dual-fuel compression ignition engines," *Energy Convers. Manag.*, vol. 251, no. August 2021, 2022.

[5] A. Katoch, A. Millán-Merino, and S. Kumar, "Measurement of laminar burning velocity of ethanol-air mixtures at elevated temperatures," *Fuel*, vol. 231, no. May, pp. 37–44, 2018.

[6] A. Montanaro and L. Allocca, "Study of Liquid and Vapor Phases of a GDI Spray," *Combust. Sci. Technol.*, vol. 191, no. 9, pp. 1600–1608, 2019.

[7] M. Xu, Y. Zhang, W. Zeng, G. Zhang, and M. Zhang, "Flash Boiling: Easy and Better Way to Generate Ideal Sprays than the High Injection Pressure," *SAE Int. J. Fuels Lubr.*, vol. 6, no. 1, pp. 137–148, 2013.

[8] M. Chang, Z. Lee, S. Park, and S. Park, "Characteristics of flash boiling and its effects on spray behavior in gasoline direct injection injectors: A review," *Fuel*, vol. 271, no. March, p. 117600, 2020.

[9] J. D. Naber and D. L. Siebers, "Effects of gas density and vaporization on penetration and dispersion of diesel sprays," *SAE Tech. Pap.*, no. 412.

[10] M. Chang, J. Hwan Park, H. Ik Kim, and S. Park, "Flash boiling macroscopic spray characteristics of multi-hole direct injection injectors with different hole arrangement," *Appl. Therm. Eng.*, vol. 170, no. December 2019, p. 114969, 2020.

[11] R. Pelé, C. Mounaïm-Rousselle, P. Bréquigny, C. Hespel, and J. Bellettre, "First Study on Ammonia Spray Characteristics with a Current GDI Engine Injector," *Fuels*, vol. 2, no. 3, pp. 253–271, 2021.

[12] E. Tinon, "Etude expérimentale des mécanismes d'atomisation effervescente. Application à la sécurité incendie dans les moteurs aéronautiques," UNIVERSITÉ DE TOULOUSE, 2018.

[13] J. Dernotte, "Influence des propriétés physico-chimiques des hydrocarbures sur l'injection et la combustion Diesel," p. 261, 2012.

[14] O. Nilaphai, C. Hespel, S. Chanchaona, and C. Mounaïm-Rousselle, "Spray and Combustion Characterization of the Alcohol Blends in the High-Pressure High-Temperature Conditions," *ILASS–Asia 2017 Oct. 18-21, 2017, Jeju, Korea Spray*, no. October, p. Oct. 18-21, 2017, 2017.

[15] N. Otsu, "A Threshold Selection Method from Gray-Level Histograms.," *IEEE Trans. Syst. Man, Cybern.*, vol. 9, no. 1, pp. 62–66, 1979.

[16] R. Privat, J. N. Jaubert, and Y. Privat, "A simple and unified algorithm to solve fluid phase equilibria using either the gamma-phi or the phi-phi approach for binary and ternary mixtures," *Comput. Chem. Eng.*, vol. 50, pp. 139–151, 2013.

[17] S. S. Sazhin *et al.*, "A simplified model for bi-component droplet heating and evaporation," *Int. J. Heat Mass Transf.*, vol. 53, no. 21–22, pp. 4495–4505, 2010.

[18] Z. Ni, C. Hespel, K. Han, and F. Foucher, "The non-ideal evaporation behaviors of ethanol/heptane droplets: Impact on diameter, temperature evolution and the light scattering by droplet at the rainbow angle," *Int. J. Heat Mass Transf.*, vol. 164, 2021.

[19] T. Eldredge and M. Thomas, "Investigation of the evaporation processes for aqueous ammonia and aqueous urea and guidelines for using simplifying assumptions," *Am. Soc. Mech. Eng. Power Div. POWER*, vol. 1, pp. 1–7, 2018, doi: 10.1115/POWER2018-7218.

[20] B. Cai *et al.*, "Energy analysis of spray flash evaporation from superheated upward jets," *Appl. Therm. Eng.*, vol. 148, no. October 2018, pp. 704–713, 2019.

[21] J. Zembi *et al.*, "Numerical Study of Ammonia Spray with a GDI Engine Injector," *SAE Tech. Pap.*, pp. 1–20, 2023.

[22] J. Zembi *et al.*, "GDI Ammonia Spray Numerical Simulation by means of OpenFOAM," *J. Ammon. Energy*, pp. 1–9, 2023.